J Bio Tribo Corros (2015) 1:2
DOI 10.1007/s40735-014-0002-8

ORIGINAL PAPER

Tribocorrosion Behavior of Duplex S/Cr(N) and S/Cr(C) Coatings on CoCrMo Alloy in 0.89 % NaCl Solution

Y. Sun · P. A. Dearnley

Received: 11 June 2014 / Revised: 12 September 2014 / Accepted: 16 September 2014 / Published online: 10 October 2014

Abstract In the present study, magnetron sputtering was used to deposit two types of duplex coatings, S/Cr(N) and S/Cr(C), onto ASTM F75 CoCrMo cast alloy, aiming at improving the tribocorrosion behavior of the medical alloy. The duplex coatings were fabricated and structured such that the inner layer comprised carbon S phase with a CoCrMo matrix by sputtering a CoCrMo alloy target in the presence of carbon containing atmosphere. The duplex coatings were found to be elastically compatible with the CoCrMo alloy, and possess higher hardness and a larger hardness-to-modulus ratio than the uncoated alloy. Tribocorrosion tests were conducted in 0.89 % NaCl solution at 37 °C under elastic contact and unidirectional sliding conditions. The results showed that the duplex S/Cr(N) coating was very effective in improving the tribocorrosion behavior of the alloy at all applied potentials, in terms of reduced friction and much improved resistance to total material loss (TML) by up to more than one order of magnitude. On the other hand, the duplex S/Cr(C) coating was effective only at open circuit and anodic potentials (APs), but not at cathodic potentials. The uncoated alloy exhibited low friction and low TML at a large cathodic potential and experienced peculiar frictional behavior at the tested AP. The results are discussed in terms of material transfer, hydrogen charging, third body effects, and synergism between wear and corrosion.

Keywords CoCrMo alloy · Tribocorrosion · Duplex coating · S phase · Friction · Wear · Corrosion

Y. Sun (✉)
School of Engineering and Sustainable Development, Faculty of Technology, De Montfort University, Leicester, UK
e-mail: ysun01@dmu.ac.uk

P. A. Dearnley
nCATS, Engineering Sciences, University of Southampton, Southampton, UK
e-mail: peter_dearnley@talktalk.net

P. A. Dearnley
Boride Services Ltd, Leeds, UK

1 Introduction

CoCrMo alloys are the most widely used metallic alloys for artificial prostheses due to their good combination of mechanical, chemical, and biomedical properties. However, there have been increasing concerns regarding the long-term durability of the joint replacement due to the generation of nano-sized particles and the release of toxic metal ions [1–3]. It has been recognized that tribocorrosion plays a very important role in degradation of CoCrMo alloys in biological environments, due to the synergistic effects between wear and corrosion [4–6]. The passive film on the bearing surface can be damaged or removed by the sliding motion between the articulating surfaces, resulting in accelerated corrosion, which can in many cases lead to accelerated wear [7, 8]. Many efforts have been made in the past decade to investigate the tribocorrosion behavior CoCrMo alloys in laboratory and simulator tests [4–6, 9–12]. An excellent review in this area has recently been provided by Mischler and Munoz [13].

Efforts have also been made in recent years to improve the tribological, corrosion, and tribocorrosion properties of biomedical alloys by surface engineering, mainly by applying an innovative surface coating [14–16] and by surface alloying [17–19]. In particular, the potential of S-phase coating and CrN coating to improve tribocorrosion behavior of biomedical alloys has been studied in details

[20, 21]. S-phase coating is an austenitic stainless steel coating supersaturated with nitrogen or carbon, possessing a high hardness (>800 Hv), excellent corrosion and tribocorrosion resistance in aqueous saline environments [20–22]. The S-phase was initially produced by low temperature nitriding or carburizing of austenitic stainless steels [23–25] and more recently of CoCr alloys with a face-centred cubic structure [17]. By magnetron sputtering a 316L stainless steel target in the presence of nitrogen or carbon containing atmospheres, S-phase coatings can be fabricated with controlled nitrogen or carbon contents [20, 21, 26]. Earlier work on S-phase coated biomedical grade stainless steel demonstrated that the S-phase coating can reduce corrosion-wear of the stainless steel, but it was not as effective as CrN coatings [21, 27]. The excellent tribocorrosion behavior of CrN coatings in biological environments has been confirmed recently in metal-on-metal hip simulator tests [14]. However, a single CrN coating on a soft substrate is prone to cracking under contact motion during tribocorrosion [27].

In the present work, magnetron sputtering was used to deposit two types of duplex coatings, S/Cr(N) and S/Cr(C), onto ASTM F75 CoCrMo cast alloy. The duplex coatings were fabricated and structured such that the inner layer comprised carbon S-phase with a CoCrMo matrix by sputtering a CoCrMo alloy target in the presence of a carbon containing atmosphere. A Cr(N) or Cr(C) coating was deposited on top of the carbon S-phase layer. The use of a Cr(C) top coating was a logical choice because the inner S-phase layer was supersaturated with carbon. The aim of this work was to evaluate the tribocorrosion behavior of the duplex coatings in comparison with the uncoated CoCrMo alloy.

2 Experimental

2.1 Material and Specimen Preparation

The substrate material used was ASTM F75 CoCrMo cast alloy which had the following nominal composition (in wt%): 28.5Cr, 6.8Mo, 0.22C, and balance Co. The material was received in the as-cast condition, which had a dendritic structure with inter-dendritic carbides. Disc specimens of 12 mm diameter and 5 mm thick were machined from the cast bar. The surface to be coated was progressively ground down to a 1200 grit finish with SiC grinding papers and then finished with a 1 μm diamond polishing cloth achieving a mirror-like surface finish of 0.03 μm (R_a), which is slightly rougher than the target finish ($R_a < 0.02$ μm) for artificial hip joints in clinic practice [28]. Prior to coating deposition, the specimens were cleaned ultrasonically in acetone for 10 min.

2.2 Duplex Coating Deposition

A laboratory scale magnetron sputtering machine was used to produce the duplex coatings. After charging with the CoCrMo alloy substrates, the deposition chamber was evacuated to a base pressure of 2×10^{-4} Pa. The substrates were then sputter cleaned for 60 min using 200 W radio frequency argon plasma at 0.93 Pa with a substrate induced self-bias of −200 V. An interfacial layer was then applied to the substrates by sputtering a CoCrMo target for 30 min in argon plasma. This was followed by the deposition of the inner carbon S-phase layer achieved by sputtering the CoCrMo target for 120 min in an atmosphere prepared by flowing Ar at 7 SCCM and CH_4 at 5 SCCM into the chamber. Finally a top layer of Cr(N) or Cr(C) was deposited by sputtering a pure Cr target for 120 min in atmospheres, respectively, containing a mixture of Ar (7 SCCM) and N_2 (5 SCCM) or Ar (7 SCCM) and CH_4 (5 SCCM). All the deposition stages were conducted with a working pressure of 0.67 Pa and an induced substrate self-bias of −50 V.

2.3 Coating Characterization

The thickness of each layer in the duplex coatings was measured using a standard ball-cratering technique, where a crater about 1 mm diameter was made by rotating a stainless steel ball of 25.4 mm diameter. Such a ball crater revealed the multilayer structure of the duplex coatings and allowed for the measurement of layer thickness. The phase constituents and crystal structure of the coatings were determined by X-ray diffraction using Cu Kα radiation. A Nanotester (Micromaterials Ltd) was used to measure the surface hardness of the specimens at five different indentation loads from 5 to 25 mN.

2.4 Tribocorrosion Testing

Tribocorrosion tests were conducted under unidirectional sliding by integrating a pin-on-disk tribometer with an electrochemical potentiostat. The experimental setup has been reported elsewhere [29]. The electrolyte used was 0.89 wt% NaCl in double distilled water. To ensure that only the specimen surface was exposed to electrochemical corrosion, the test cell, the pin (ball) holder, and all other fixtures were made of inert insulating materials. The sliding contact pin was an inert sintered alumina ball of 8 mm diameter. Before the test, the coated and uncoated specimens were masked using insulating lacquer leaving a test area of 11 mm diameter exposed to the electrolyte. The reference electrode was a saturated calomel electrode (SCE) inserted into the test cell containing 250 ml electrolyte; the auxiliary electrode was a platinum wire. All

tests were conducted in open air at a temperature of 37 °C, controlled by an external heating reservoir.

Anodic polarization tests were initially carried out while the specimen was rotating at a speed of 60 rpm without contacting the alumina ball against the coated or uncoated specimen. To standardize and clean the surface, the coated and uncoated specimens were cathodically polarized at −900 mV(SCE) for 180 s and then rested (stabilized) at open circuit for 600 s. Anodic polarization was then started from −200 mV(SCE) versus OCP at a scan rate of 1 mV s^{-1} until a current density of 1 mA cm^{-2} was reached. It should be pointed out that the surface condition during the present potentiodynamic measurements under rotation is different from that under a stationary state because of the surface changes induced by the mechanical actions.

Tribocorrosion testing was conducted by applying a constant load of 1 N to the Al_2O_3 ball and making it slide against the coated or uncoated specimens at 60 rpm for 7200 s. Hertz elastic contact analysis indicated that the initial contact pressure was ∼630 MPa with a contact radius of 27 μm for Al_2O_3 on uncoated Co–Cr–Mo with a maximum shear stress of 197 MPa at a depth of 13 μm below the surface. Such contact stresses are much greater than those between 14 and 60 MPa estimated to act on the bearing surfaces of artificial hip joints [13, 30]. Given that the uniaxial and shear yield strengths of CoCrMo alloy are about ∼500 and 250 MPa, respectively, a maximum shear stress of 197 MPa was not sufficient to cause bulk plastic deformation according to the Tresca criterion. Plastic deformation, if any, should be mainly confined to the asperity level.

Four tribocorrosion conditions were applied to each coated and uncoated CoCrMo specimen under: (a) open circuit potential (OCP); (b) constant cathodic potential [at −950 and −600 mV(SCE)]; (c) constant anodic potential (AP) [at 100 mV(SCE)]. In all tests, the corrosion-wear track diameter was 6 mm. Before sliding contact commenced, the specimen was standardized by cathodic polarizing at −900 mV(SCE) for 180 s, followed by resting at the set potentials for 600 s under rotation-only condition. After sliding for 7200 s, test-pieces were rested at their respective potentials for further 600 s under the rotation-only condition. The OCP (or current) and coefficient of friction (COF) were recorded continuously before, during, and after sliding. Each test was duplicated and the averaged results recorded.

After tribocorrosion testing, the volume loss of material from each corrosion-wear track [total material loss (TML)] was evaluated by measuring the surface profile across the track at four equally spaced locations using a contacting surface profilometer (Mitutoyo SJ400). The surface morphology of the corrosion-wear tracks were subsequently examined by light-optical and scanning electron microscopy (SEM).

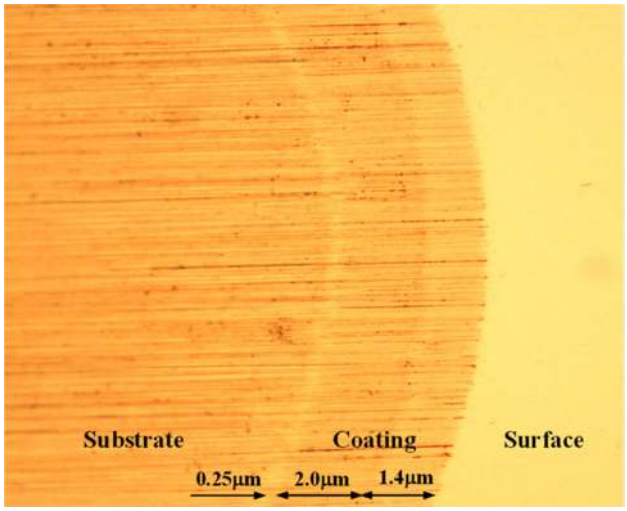

Fig. 1 A ball crater made on the S/Cr(N) coating surface, revealing the interfacial bond layer, the inner S-phase layer, and the outer Cr(N) layer

3 Results

3.1 Coating Thickness and Hardness

Figure 1 shows part of a ball crater made on the S/Cr(N)-coated surface revealing the duplex coating and substrate. The test coatings had a multilayer structure which comprised an interfacial bond layer of Co–Cr–Mo 0.25 μm thick, a carbon S-phase inner layer 2.0 μm thick, and an outer Cr(N) or Cr(C) layer 1.4 μm thick. Table 1 summarizes the hardness (H) and reduced modulus (E_r) values, as well as the calculated H/E_r ratios, obtained for the coated and uncoated specimens under five indentation loads. The hardness value from 7 to 8 GPa for the uncoated CoCrMo alloy are significantly higher than those recorded using microhardness testing methods (typically ∼3.5 GPa), although they do agree with other reports of nanoindentation hardness determined for this material [14]. Moreover, the nanohardness decreased with increasing load. Both observations are indicative of strain hardening of the surface and near surface as a result of mechanical polishing and the formation of a Beilby layer. The scatter in nanohardness was also narrow, indicating no differentiation between the very hard interdendritic carbides (∼10–12 GPa) and the dendritic solid solution (Co–Cr–Mo) phase (∼2 GPa), further supporting the hypothesis that a separate work hardened layer had been smeared over the surfaces of the micro-constituent phases of the material.

Table 1 Surface hardness and reduced modulus, measured by nanoindention at various loads

Indentation load (mN)	Hardness (GPa)			Reduced modulus (GPa)			H/E_r ($\times 10^{-3}$)		
	Uncoated	S/Cr(N)	S/Cr(C)	Uncoated	S/Cr(N)	S/Cr(C)	Uncoated	S/Cr(N)	S/Cr(C)
5	9.84	17.64	14.78	252.17	269.89	240.99	39.02	65.36	61.33
10	8.32	17.94	15.98	241.24	257.73	242.96	34.49	69.61	65.65
15	8.20	18.18	15.15	232.03	259.41	230.75	35.34	70.08	67.17
20	7.21	18.23	14.94	222.85	248.43	225.41	32.35	73.38	66.28
25	7.01	17.53	14.79	222.33	240.02	220.30	31.53	73.04	67.14

From Table 1 it is apparent that the duplex coatings possessed higher hardness than the uncoated specimen, about 15 GPa for the S/Cr(C) coating and 18 GPa for the S/Cr(N) coating, the latter being about 20 % harder than the former. It is also important to note that the reduced moduli of the duplex coatings were similar to those of the uncoated specimen, indicating that there was little elastic mismatch between the coatings and the substrate. Elastic compatibility between coating and substrate is important in tribological coating systems in order to minimize stress concentration at the coating–substrate interface. The higher hardness of the coatings, particularly the S/Cr(N) system, also resulted in a larger *H*/*E* ratio than the uncoated specimen (see Table 1). A higher *H*/*E* ratio is preferred for wear resistance since it promotes asperity elastic deformation rather than plastic deformation [31]. Thus, the created duplex coatings are good candidates for the CoCrMo alloy from a contact mechanics point of view.

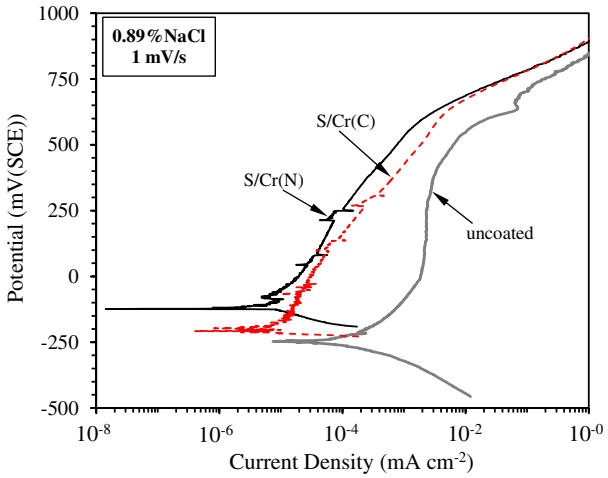

Fig. 2 Potentiodynamic polarization curves recorded for the test specimens under rotation-only (60 rpm) condition without sliding (no contact between the specimen and the alumina ball)

3.2 Corrosion Behavior of Duplex Coatings

Figure 2 shows the potentiodynamic polarization curves for the three coated and uncoated specimens measured at 37 °C under rotation-only condition (without sliding contact). The uncoated specimen showed a corrosion potential about −250 mV(SCE) and spontaneous passivation behavior at APs above the corrosion potential with a passivity current density about 2×10^{-3} mA cm^{-2} in the plateau region. Transition from passive to transpassive behavior occurred at the breakdown potential about 550 mV(SCE) due to oxygen evolution and significant thickening of the oxide film, which is normally accompanied with a change in film composition and an increased dissolution rate. The small secondary peak occurring at the potential about 650 mV(SCE) was believed to be due to the oxidation of chromium [32].

For the duplex coatings, the corrosion potentials were shifted anodically; this was most significant for the S/Cr(N) system. The duplex coatings showed anodic current densities one to two orders of magnitude lower than that of the uncoated specimen. These demonstrated the excellent corrosion resistance of the duplex coatings in the saline test solution. Of the two duplex coatings, the S/Cr(N) system was more corrosion resistant with passivity current densities as low as 10^{-5} mA cm^{-2}. It was also noted that the anodic part of the curves of the duplex coatings contained a few current fluctuations and spikes at potentials below 300 mV(SCE), which could be explained by the existence of pinholes in the outer Cr(N) or Cr(C) coating.

3.3 Sliding at OCP

Sliding tests were first conducted at open circuit without externally applied potentials. The evolution of OCP before, during, and after sliding is shown in Fig. 3a. During the first 600 s, the specimens were rotating-only without contact with the slider. The duplex-coated specimens had an OCP that was about 200 mV higher than the uncoated specimen. Upon sliding, all specimens experienced a significant drop in OCP—a common phenomenon in this type of testing [33]. During the sliding period of 7200 s, OCP

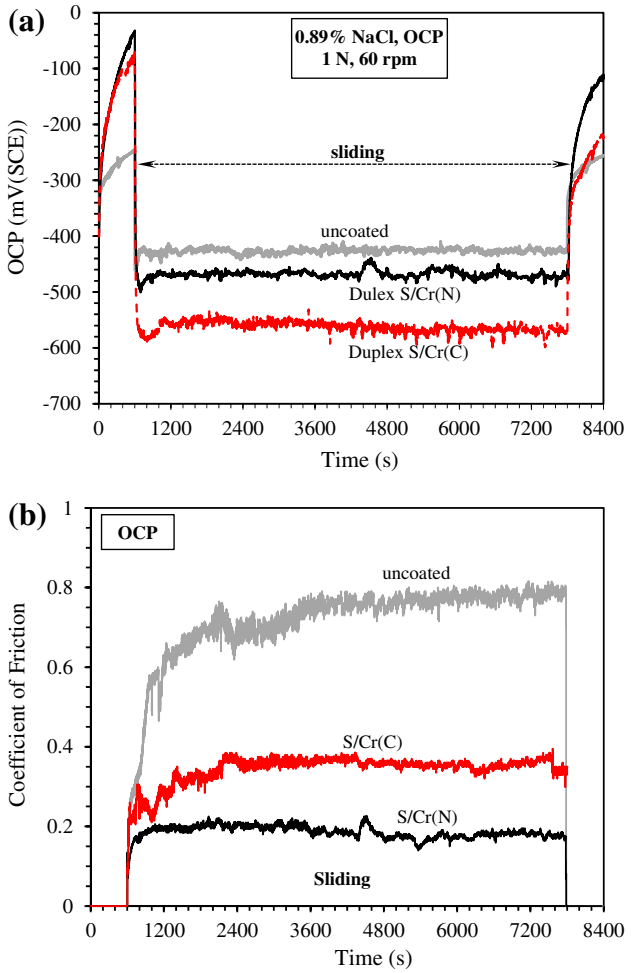

Fig. 3 Open circuit potential recorded before, during, and after sliding under open circuit condition (**a**) and COF curve recorded during sliding at OCP (**b**)

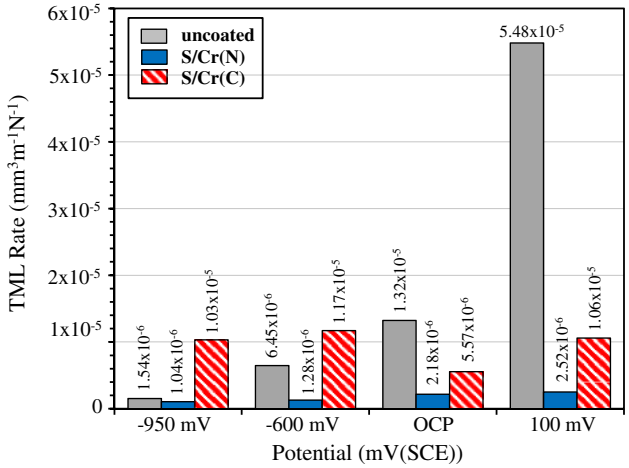

Fig. 4 Specific total material loss (TML) rate as a function of applied potential. Test condition: 1 N, 60 rpm, 37 ± 0.5 °C, 0.89 wt% NaCl, 7,200 s

for all specimens continued to decrease slightly due to an increased corrosion-wear track area. At the termination of sliding, OCP increased rapidly for the first few seconds and then gradually (after several minutes) approached the original value.

Rather surprisingly, the cathodic drop in OCP during sliding was more significant for the coated specimens than for the uncoated specimen. A drop in OCP by about 500 and 400 mV(SCE) was observed, respectively, for the S/Cr(C) and S/Cr(N) coating as compared to about 180 mV(SCE) for the uncoated specimen. Although it has been proposed that a larger drop in OCP during sliding can result in larger TML [33], in the present work, the degree of cathodic shift in OCP did not seem to be proportional to the measured TML (discussed in Sect. 4). The larger drop in OCP during sliding for the duplex coatings suggests that the coating surface may have different composition from the interior of the coating. Detailed chemical profiling analysis is required to confirm such a proposition.

Figure 3b shows the COF recorded during sliding at OCP. The duplex S/Cr(N) coating exhibited a COF value <0.2 throughout the sliding period, while the uncoated specimen had a COF that rose steadily through the test reaching a maximum of 0.8. No correlation was observed between COF (Fig. 3b) and the fall in OCP (Fig. 3a).

Surface profiles were measured across the corrosion-wear tracks generated with various potentials. Such tracks were used to estimate the TML—this data was then normalized with the contact load (1 N) and the total sliding distance (135.7 m) to obtain the specific TML rates (TMLR) ($mm^3\ m^{-1}\ N^{-1}$). This data is summarized in Fig. 4.

Under OCP conditions the application of the duplex S/Cr(C) coating to Co–Cr–Mo reduced the TMLR by 2.4 times compared to the uncoated material, while an order of magnitude reduction in TMLR was observed for the duplex S/Cr(N) coated Co–Cr–Mo and the friction was also lower (Fig. 4).

To reveal the depth of the wear track in the duplex coatings, a ball crater was made on each corrosion-wear track (Fig. 5). It was clear that material loss was confined to the outer Cr(N) or Cr(C) coatings—here, about 0.15 and 0.4 μm, respectively, had been removed from the coatings. No evidence of wearing-through, debonding, and cracking of the coatings could be seen.Microscopic examination of the corrosion-wear tracks on the uncoated specimen (Fig. 6) revealed many deep and wide abrasion marks (grooves) whereas the contact surface of the alumina balls appeared to be covered in transferred material. The corrosion-wear tracks of the duplex-coated specimens were less severely damaged. The track on

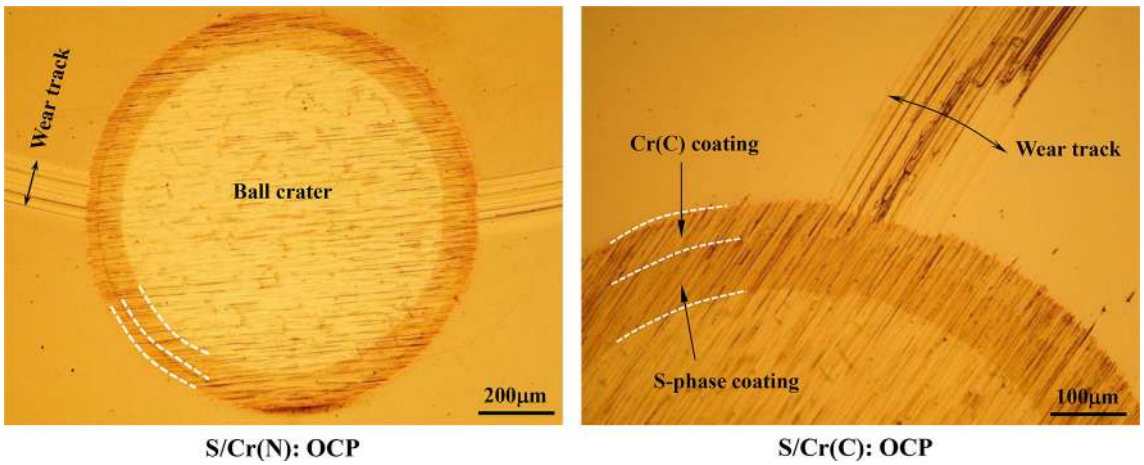

Fig. 5 Ball craters made on the wear tracks generated by sliding wear at OCP on the duplex S/Cr(N) and S/Cr(C) coatings, showing wear depth relative to coating thickness. The *dotted lines* were drawn to aid reader's eye in distinguishing the duplex coatings

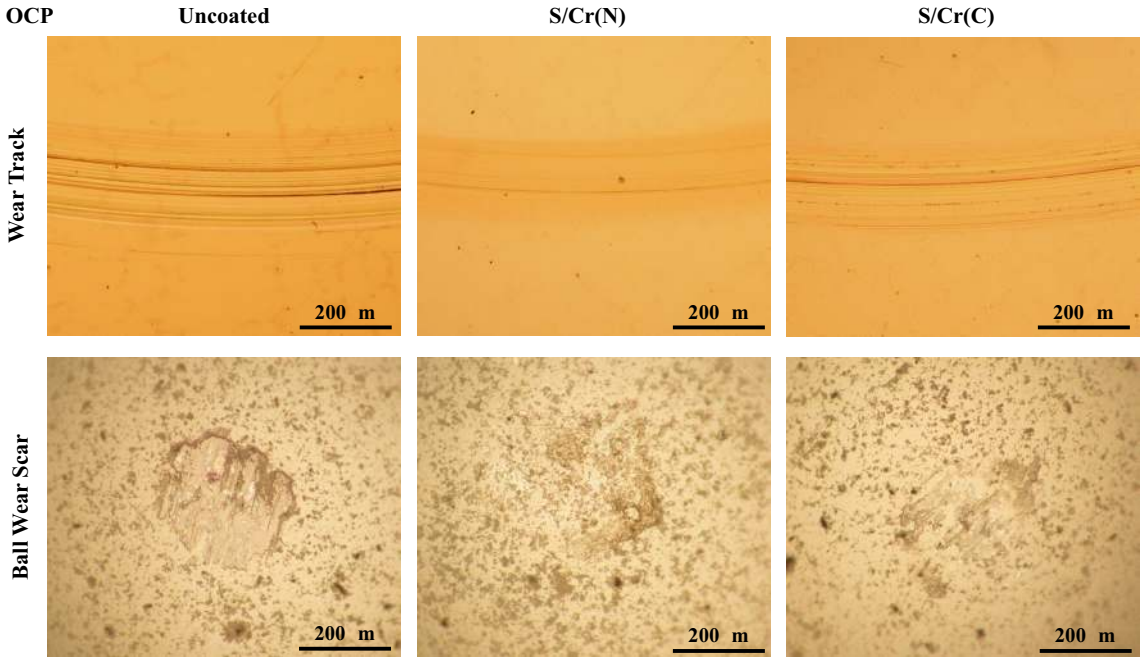

Fig. 6 Wear track and ball wear scar morphologies after sliding wear testing at OCP in 0.89 % NaCl, at 1 N and 60 rpm for 7,200 s

the S/Cr(C)-coated specimen showed only slight scratching, while the S/Cr(N)-coated specimen showed a track with a polished appearance. For both coated specimens the corresponding alumina ball counterface surfaces were observed to be covered, at least in part, with transferred material from the corrosion-wear tracks. The grooving and polishing effects are probably due to a combination of anodic dissolution and micro-asperity shearing, as observed on similarly tested coated austenitic stainless steels [34]. Polishing may also be due to micro-abrasion, but the source of a likely abrasive material is not clear.

3.4 Sliding at Cathodic Potentials (CP)

Testing with a CP of −950 and −600 mV(SCE), resulted in negative current densities of about 0.15 mA cm^{-2} and 0.005–0.06 mA cm^{-2}, respectively, for all three test specimens. There was no sharp change in the measured cathodic current on commencement of sliding contact, indicating there was little mechanical influence on the kinetics of the cathodic reaction(s).

With a CP of −950 mV(SCE), the test specimens showed different frictional behavior, see Fig. 7a. Due to the absence of a passive film on the wear track, the

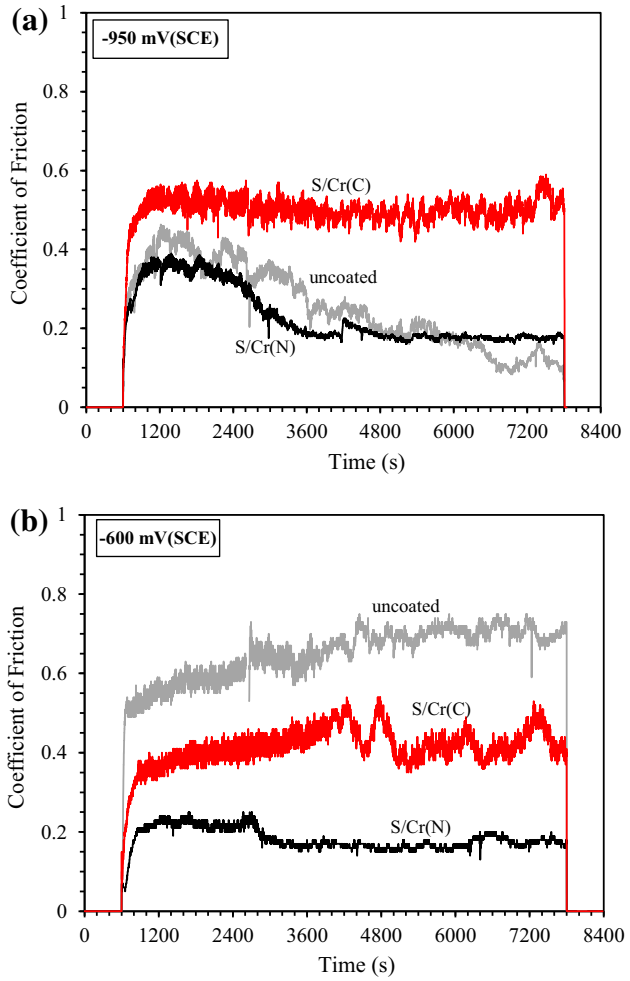

Fig. 7 Coefficient of friction recorded during sliding under potentiostatic condition at cathodic potentials: **a** −950 mV(SCE) and **b** −600 mV(SCE)

S/Cr(N) coating had a relatively high COF (about 0.35) during the first 2,000 s sliding, after which its COF decreased to values similar to those measured at OCP. On the other hand, the COF of the S/Cr(C) coating was the highest throughout the sliding period with values around 0.5. Most interestingly, the COF of the uncoated specimen was significantly reduced as compared to that measured at OCP. As can be seen from Fig. 7a, the COF of the uncoated specimen decreased with sliding time such that during the final 1,000 s sliding, its value was even lower than that of the S/Cr(N) coating. It thus seems that cathodic protection was very effective for the uncoated specimen in terms of friction reduction. However, such a cathodic protection depended on the applied CP. As shown in Fig. 7b, at a lower CP of −600 mV(SCE), the general friction behavior of all test specimens was different from that observed at −950 mV(SCE), but was rather similar to that observed at OCP in Fig. 3b.

The TMLR of the uncoated specimen was reduced significantly at −950 mV(SCE), by nearly an order of magnitude as compared to that measured at OCP (Fig. 4). To a lesser extent, the duplex S/Cr(N) coating also experienced a reduction in TMLR at −950 mV(SCE) as compared to that measured at OCP. Rather surprisingly, the duplex S/Cr(C) behaved differently: its TMLR was increased significantly by about 100 % when potential was changed from OCP to −950 mV(SCE).

Figure 8 shows microscopic images of the corrosion-wear tracks and ball wear scars produced at −950 mV(SCE). The track on the uncoated specimen was narrow and smooth with a few isolated scratch marks caused by the isolated debris transferred to the ball. The track on the S/Cr(N) coating again showed a smooth polished appearance. On the other hand, a much wider corrosion-wear track with many deep scratch marks was produced on the S/Cr(C) coating. Some of the scratches were as deep as 1.3 μm and nearly penetrated the outer 1.4-μm-thick Cr(C) layer, obviously caused by the large amount of material transferred to the alumina ball (Fig. 8).

Since the tests at −950 mV(SCE) showed unusual friction and wear behavior, further tests were conducted at a much reduced CP, −600 mV. From Fig. 4, it can be seen that as compared to those measured at −950 mV(SCE), the TMLR measured at −600 mV(SCE) was increased, only marginally for the duplex coated specimens, but significantly for the uncoated specimen by several times. Microscopic examination showed that the corrosion-wear track produced on the uncoated specimen was wider and rougher than that produced at −950 mV(SCE). A larger amount of material transfer to the alumina ball was also observed. Again, the corrosion-wear track produced on the S/Cr(N) coating at −600 mV(SCE) was smooth with a polished appearance. Sliding at −600 mV(SCE) also resulted in a wide and deep corrosion-wear track on the S/Cr(C) coating, with a large amount of material transferred to the ball.

3.5 Sliding at Anodic Potential (AP)

At an AP of 100 mV(SCE), which fell in the passive region for all three specimens, the current decreased with time for the first 600 s without sliding, due to thickening of the oxide film (Fig. 9a). Upon sliding, the current increased abruptly and maintained at relatively high values during the sliding period until the termination of sliding, then the current decreased quickly due to repassivation of the wear track area. From Fig. 9a, it can be seen that the uncoated specimen experienced a much larger increase in current during sliding than the coated specimens. In particular, the S/Cr(N) duplex coating exhibited the lowest increase in current during sliding: 18 times lower than the uncoated

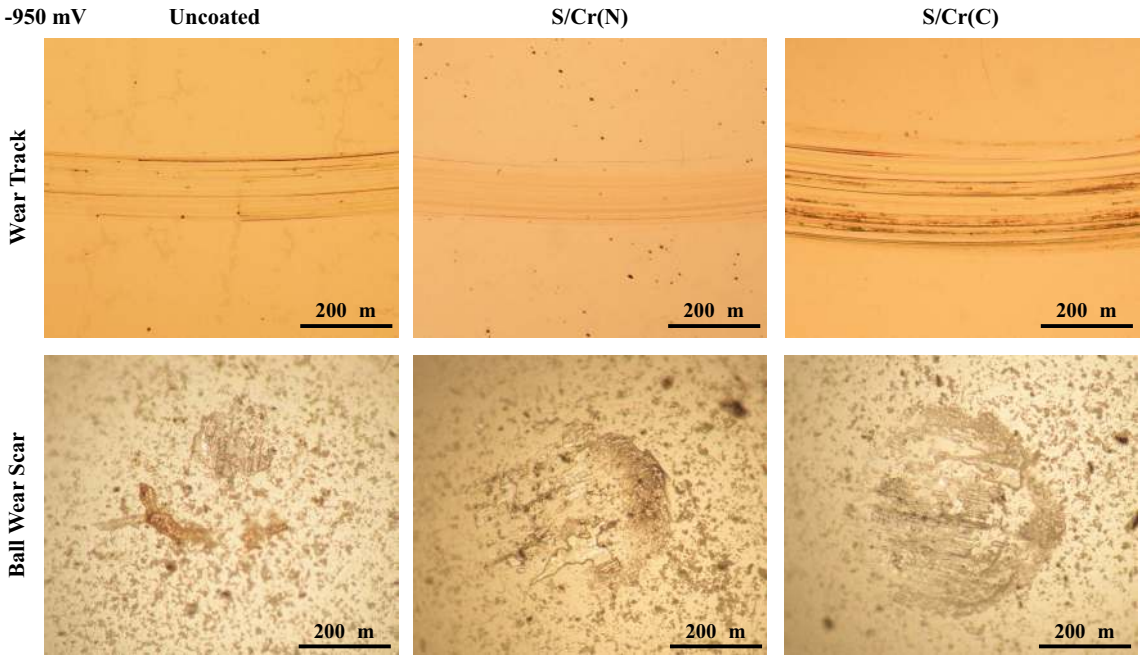

Fig. 8 Wear track and ball wear scar morphologies after sliding wear testing at −950 mV(SCE) in 0.89 % NaCl, at 1 N and 60 rpm for 7,200 s

specimen. For the coated specimens, the current increased steadily with increasing sliding time. But for the uncoated specimen, the current fluctuated largely with many sharp spikes during sliding. It is also noted from Fig. 9a that for the S/Cr(N) coating, the current decreased just after starting sliding, which could be due to the rotation motion and the change in composition of the coating from surface to the interior. This is an issue that deserves further investigation through mass transport and chemical analysis.

Compared to those measured at OCP (Fig. 3b), the COF values of all specimens measured at 100 mV(SCE) were reduced (Fig. 9b), presumably due to the repeated formation of an oxide film in the wear track. The reduction in COF was initially the most significant for the uncoated specimen: its COF value was reduced from about 0.75 at OCP to about 0.35 at 100 mV(SCE) for the first 5,500 s sliding. It is also interesting to note that after about 5,500 s sliding, the COF of the uncoated specimen started to increase, gradually approaching values higher than 1. Such an unusual phenomenon will be discussed in Sect. 4.2.

At the AP of 100 mV(SCE), a significant increase in TMLR was observed for the uncoated specimen as compared to those measured at other potentials (see Fig. 4), while the S/Cr(N) coating only experienced a marginal increase in TMLR over that measured at OCP. For the S/Cr(C) coating, the TMLR at 100 mV(SCE) was similar to those measured at CP but was larger than that measured at OCP. The corrosion-wear tracks produced on both duplex coatings at 100 mV(SCE) were very smooth with a polished appearance (Fig. 10), while that produced on the uncoated specimen was much deeper with some dark areas near the edges of the track (see Fig. 10). Another distinct feature observed at 100 mV(SCE) was that material transfer to the alumina ball was minimal in the cases of the two duplex coatings.

3.6 Effect of Electrochemical Potential on Friction and TMLR

The dependence of average COF on applied potential is shown in Table 2. The S/Cr(N)-coated specimen displayed remarkably low friction (COF < 0.2) at all applied potentials, whereas slightly higher friction values were evident for the S/Cr(C)-coated specimen; in both cases the COF decreased progressively with increasing applied potential. The trend for the uncoated Co–Cr–Mo test-pieces was more erratic (Table 2), low friction ($\sim$0.2) only being observed at CP of −950 mV(SCE), very much higher COF values ($\sim$0.5–0.6) being recorded at the other potentials.

From Fig. 4, it can be seen that the TMLR of the uncoated specimen and the S/Cr(N) coating increased with increasing potential: such an increase was much more significant for the uncoated specimen than for the duplex coating. The TMLR of the uncoated specimen was increased by 35 times when the potential was increased from −950 to 100 mV(SCE), while the S/Cr(N) coating only registered an increase in TMLR by about 2.5 times. A similar phenomena have been observed for uncoated CoCrMo [35] and nitrided Ni–Cr alloys [18]. For the duplex S/Cr(C) coating, no clear trend could be found

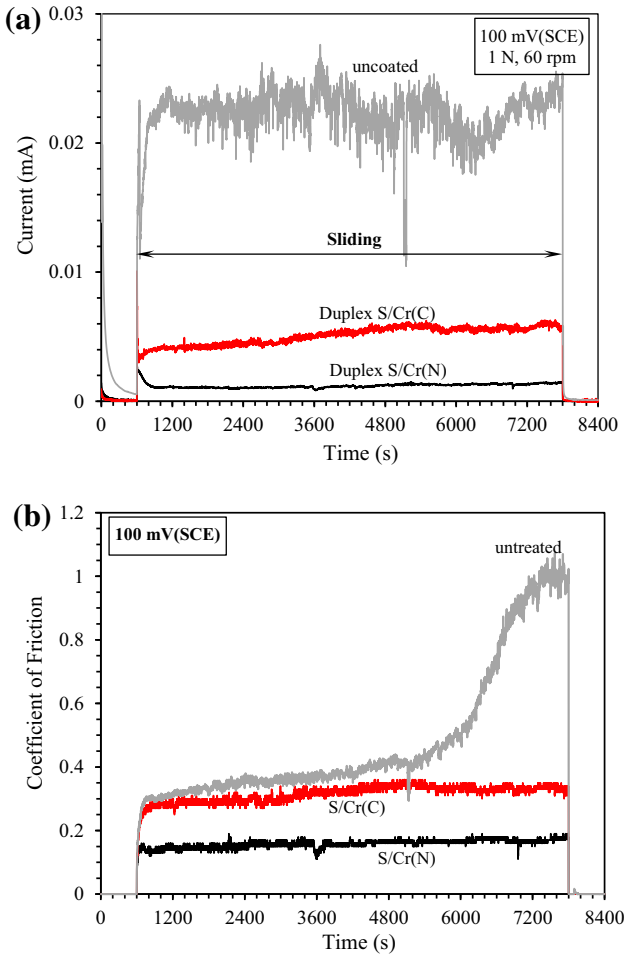

Fig. 9 Anodic current (**a**) and COF (**b**) recorded during sliding under potentiostatic condition at 100 mV(SCE)

between TMLR and applied potential. From Fig. 4, it can also be seen that the duplex S/Cr(N) coating was very effective in improving the TML resistance of the CoCrMo alloy at all potentials and the degree of improvement increased with increasing potential. On the other hand, the duplex S/Cr(C) coating was only effective at OCP and the AP, but became ineffective at cathodic potentials.

4 Discussion

The experimental work presented in the previous section has led to some interesting observations that deserve further discussion. These include the strong dependence of the tribocorrosion behavior of the uncoated specimen on applied potential, the peculiar behavior of the duplex S/Cr(C) system at cathodic potentials, and more importantly the excellent tribicorrosion behavior of the duplex S/Cr(N) system in terms of much reduced friction and improved resistance to TML. These phenomena can be explained by the third body effect, material transfer, hydrogen charging, formation and deposition of corrosion products, and synergism between wear and corrosion, as follows.

4.1 Effect of Cathodic Potentials on Friction and TML

It has been reported by many investigators that TML from the corrosion-wear track during tribocorrosion is the result of chemical wear (V_{chem}) and mechanical wear (V_{mech}) [36]. The purpose of conducting wear tests at cathodic potentials is to determine the pure mechanical wear component of the test specimens [7, 36, 37]. The selection of a cathodic potential for the test is rather arbitrary in the literature although some investigators have suggested that hydrogen charging should be considered because this can cause hydrogen embrittlement [13, 38]. Unfortunately, very little work has been reported regarding the effect of varying cathodic potentials on friction and TML of CoCrMo alloy. The present work clearly showed that friction and TML of the uncoated specimen strongly depended on the chosen cathodic potentials, as evidenced by the test results at −950 and −600 mV(SCE) (Fig. 4; Table 2). An interesting question is thus raised as to why at −950 mV(SCE) the uncoated specimen experienced much lower friction and TMLR than at −600 mV(SCE) and at OCP. The large difference in mechanical wear component between CP and AP has been observed by several investigators in several alloy systems including CrCoMo alloy [13, 35]. It has been proposed that the presence of a passive film at AP could interfere with dislocation mobility and thus could cause embrittlement of the test surface and lead to larger mechanical wear [39, 40]. Since a passive film is not expected to form at both CP tested in the present work, another possible explanation can be derived from the effect of hydrogen charging. The equilibrium potential for hydrogen evolution in such a neutral solution was estimated to be about −650 mV(SCE). Hydrogen evolution was thus expected at −950 mV(SCE) but not at −600 mV(SCE). Although hydrogen charging can cause embrittlement of the test surface, it may not be always detrimental to tribological properties. In a recent study by Pokhmurskii et al. [41], it was found that after electrolytic hydrogenation, α-titanium possessed increased surface hardness and much reduced friction, although its ductility was reduced. The reduced friction was believed to result from the change of asperity deformation from plastic to elastic after hydrogenation [41]. The same situation may also apply in the present uncoated specimen. Indeed, the corrosion-wear track produced at −950 mV(SCE) showed a micro-polishing feature with limited plastic deformation (Fig. 8), while that produced at −600 mV(SCE) showed many deep and

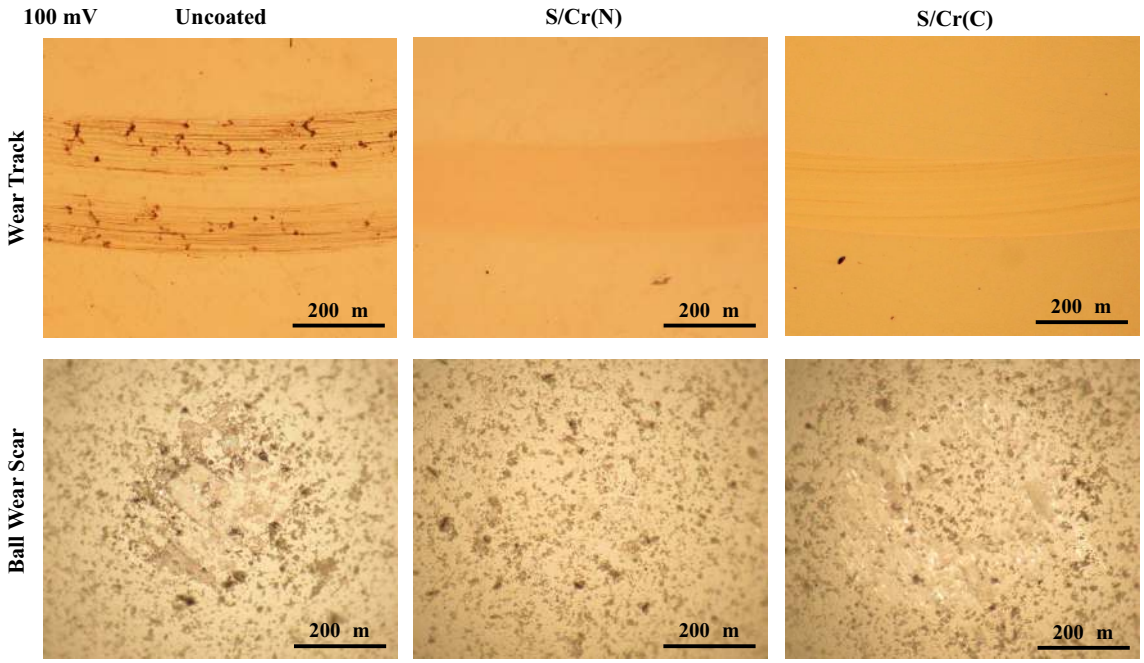

Fig. 10 Wear track and ball wear scar morphologies after sliding wear testing at 100 mV(SCE) in 0.89 % NaCl, at 1 N and 60 rpm for 7,200 s

Table 2 Average coefficient of friction values as a function of potential

Potential [mV(SCE)]	COF		
	Untreated	S/Cr(N)	S/Cr(C)
−950	0.25	0.23	0.49
−600	0.65	0.18	0.41
OCP	0.72	0.19	0.34
100	0.49	0.16	0.32

wide abrasion marks which are clear signs of surface plastic deformation.

Another problem associated with CP tests is that due to the absence of a passive film on the surface, material transfer from the corrosion-wear track to the slider may become prominent, which can result in increased TMLR as observed previously in [29] for low temperature plasma carburized 316L steel. The same problem has also been encountered in the present work for the duplex S/Cr(C) coating, which showed increased TMLR at cathodic potentials (Fig. 4). Such a peculiar behavior can be explained by the significant amount of material transferred to the alumina ball as shown in Fig. 8. These transferred material served as abrasives to produce many deep and wide abrasion marks on the wear track and cause accelerated TML. Thus it was difficult to determine the "pure mechanical wear" of this duplex coating under the present testing conditions. However, the same problem did not seem to happen for the duplex S/Cr(N) coating which

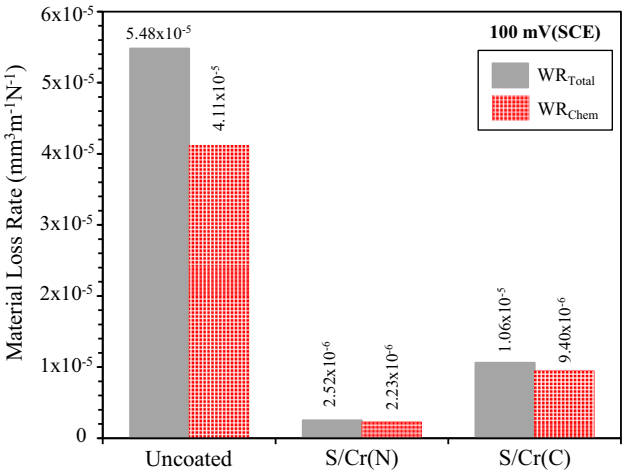

Fig. 11 Measured TML rate and calculated chemical wear rate for the specimens tested at the anodic potential of 100 mV(SCE) in 0.89 wt% NaCl at 1 N and 60 rpm for 7,200 s

showed the expected gradual decrease in TMLR and increase in friction as potential was reduced (Fig. 4; Table 2). The higher hardness and larger *H*/*E* ratio of the S/Cr(N) coating could provide better resistance to abrasion by the transferred material.

4.2 Contribution of Chemical Wear to TML at Anodic Potential

Since the anodic current was recorded during each sliding test at 100 mV(SCE), the chemical component (V_{chem})

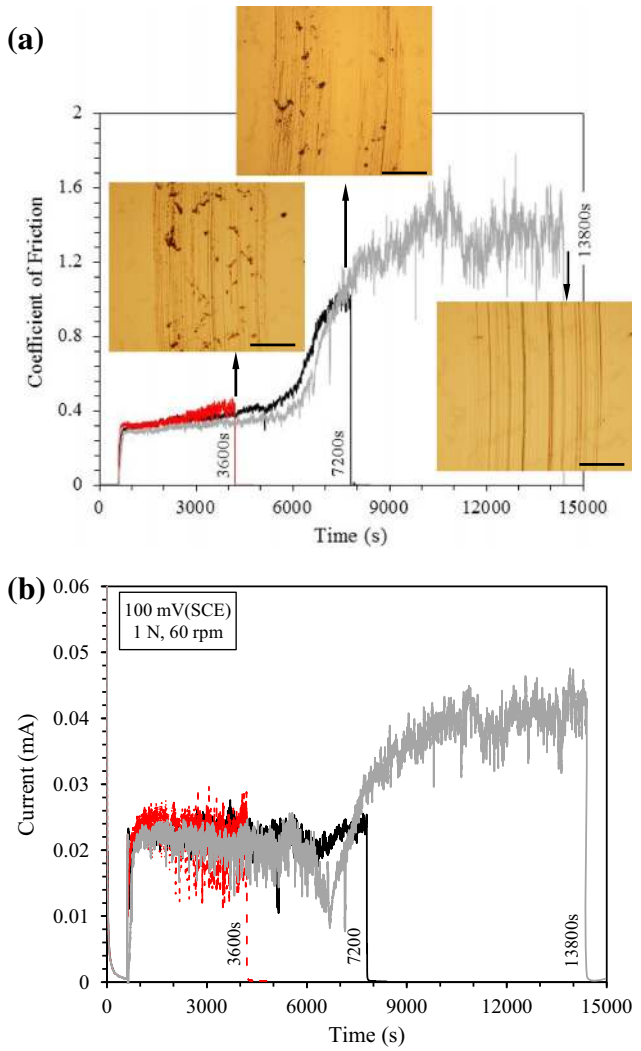

Fig. 12 COF recorded during sliding wear of the uncoated specimen under potentiostatic condition at 100 mV(SCE) for different durations and the morphologies of the generated wear tracks (**a**) and anodic currents recorded during the same sliding periods (**b**)

could be estimated according to Faraday's law [7, 8]. In the calculation, the valence of corrosion was assumed to be 3 to account for chromium oxide film formation. The results in Fig. 11 show that chemical wear had a major contribution to TML in all tested specimens. In the case of the duplex-coated specimens, nearly 90 % of TML was due to chemical wear. Thus the principal mechanism of TML was the cyclic formation and then removal of the oxide film, with limited mechanical wear of the coating itself. This agreed well with the observed smoothness and polished-like surface appearance of the wear tracks (see Fig. 10). Such a situation is similar to electrochemical-mechanical polishing which is based on the principle of repeated formation and then removal of a passive film under combined electrochemical and mechanical actions, resulting in a polished surface [42].

The uncoated specimen exhibited erratic friction behavior at 100 mV(SCE) in that its COF started to increase after 5,500 s sliding, as shown in Fig. 9b. It is thus imperative to conduct further tests at 100 mV(SCE) for different durations: one for 3,600 s sliding before the rise in COF and another for 13,800 s sliding after the increase in COF. Figure 12a shows the COF curves recorded during sliding for three different durations, together with microscopic images of the corrosion-wear tracks. Before the rise in COF (3,600 s), the track contained many dark areas which were most likely deposited corrosion products. During the course of increasing COF (7,200 s), the dark areas were removed from the central part of the track. In the high COF region (13,800 s), no such dark areas were found in the track. It is thus obvious that the deposition of corrosion products onto the corrosion-wear track was responsible for the low friction for the first 5,500 s sliding and the removal of the corrosion products led to the transition from low friction to high friction.

The deposition of corrosion products onto the corrosion-wear track also affected the evolution of anodic current as shown in Fig. 12b. After 7,200 s sliding when there were no dark areas in the track, the anodic current was increased to a higher level. This also resulted in an increase in the contribution of chemical wear to TML from the corrosion-wear track. It can be concluded that the deposition of corrosion products not only reduced friction but also reduced metal dissolution from the corrosion-wear track on the uncoated specimen.

4.3 Beneficial Effects of Duplex S/Cr(N) Coating

The experimental results demonstrated that the duplex S/Cr(N) coating was very effective in improving the tribocorrosion behavior of the CoCrMo alloy at all tested potentials. The beneficial effects of such a duplex coating include low friction, low TML, low mechanical wear, low chemical wear, a smooth wear track appearance, and much reduced material transfer to the slider. These beneficial effects can be explained by the high hardness, large H/E ratio (Table 1), and excellent corrosion resistance (Fig. 2) of the coating. The high coating hardness is beneficial in reducing mechanical wear because it provides better resistance to abrasion caused by the slider, trapped wear particles, and transferred material. The large H/E ratio helps to reduce asperity plastic deformation such that wear proceeds in a micro-polishing mode at all potentials, resulting in a polished surface appearance. The enhanced corrosion resistance is associated with the very low passivity current density (Fig. 2) such that wear-accelerated corrosion is much reduced during sliding (Fig. 9a). The smaller corrosion-wear track area also contributes to the reduced rise in current during sliding. In addition, asperity

elastic deformation promoted by the large *H*/*E* ratio would minimize damages to the oxide film and thus reduce chemical wear.

5 Conclusions

(1) Duplex S/Cr(N) and S/Cr(C) coatings have been successfully deposited on CoCrMo alloy with enhanced surface hardness and increased hardness-to-modulus ratio. The duplex S/Cr(N) coating possesses higher hardness and larger hardness-to-modulus ratio than the duplex S/Cr(C) coating.

(2) The duplex S/Cr(N) coating is very effective in improving the tribocorrosion behavior of the CoCrMo alloy in 0.89 % NaCl solution at all tested electrochemical potentials, in terms of reduced friction and enhanced resistance to material removal from the wear track.

(3) The duplex S/Cr(C) coating can improve the tribocorrosion behavior of the CoCrMo alloy only at OCP and AP, but not at cathodic potentials where a large amount of material transfer to the slider causes accelerated mechanical wear from the S/Cr(C) coating.

(4) The tribocorrosion behavior of the uncoated CoCrMo alloy is very much potential-dependent. At large cathodic potentials [e.g., −950 mV(SCE)] the uncoated CoCrMo alloy exhibits both low friction and low TMLR.

(5) At the AP of 100 mV(SCE), the uncoated specimen shows a transition from low friction to high friction, and chemical wear is predominant during sliding of the duplex coatings where material loss is caused by the periodic formation and removal of the oxide film.

Conflict of interest On behalf of all authors, the corresponding author states that there is no conflict of interest.

References

1. Smith AJ, Dieppe P, Vernon K, Porter M, Blom AW (2012) Failure rates of stemmed metal-on-metal hip replacements: analysis of data from the National Joint Registry of England and Wales. Lancet 379:1199–1204
2. MacDonald SJ (2004) Can a safe level for metal ions in patients with metal-on metal total hip arthroplasties be determined? J Arthroplast 19:71–77
3. Germain MA, Hatton A, Williams S, Matthews JB, Stone MH, Fisher J, Ingham E (2003) Comparison of the cytotoxicity of clinically relevant cobalt–chromium and alumina ceramic wear particles in vitro. Biomaterials 24:469–479
4. Mathew MT, Runa MJ, Laurent M, Jacobs JJ, Rocha LA, Wimmer MA (2011) Tribocorrosion behavior of CoCrMo alloy for hip prosthesis as a function of loads: a comparison between two testing systems. Wear 271:1210–1219
5. Yan Y, Neville A, Dowson D (2007) Tribo-corrosion properties of cobalt-based medical implant alloys in simulated biological environments. Wear 263:1105–1111
6. Yan Y, Neville A, Dowson D, Williams S, Fisher J (2010) Electrochemical instrumentation of a hip simulator: a new tool for assessing the role of corrosion in metal-on-metal hip joints. Proc Inst Mech Eng H 224:1267–1273
7. Landolt D, Mischler S, Stemp M (2001) Electrochemical methods in tribocorrosion: a critical appraisal. Electrochim Acta 46:3913–3929
8. Ponthiaux P, Wenger F, Drees D, Celis JP (2004) Electrochemical techniques for studying tribocorrosion processes. Wear 256: 459–468
9. Swaminathan Viswanathan, Gilbert JeremyL (2012) Fretting corrosion of CoCrMo and Ti6Al4V interfaces. Biomaterials 33:5487–5503
10. Mathew MT, Wimmer MA (2013) Tribocorrosion in artificial joints: in vitro testing and clinical implications. In: Yan Y (ed) Bio-tribocorrosion in biomaterials and medical implants. Woodhead, Cambridge, pp 341–371
11. Yan Y, Neville A (2013) Bio-tribocorrosion: surface interactions in total joint replacement (TJR). In: Yan Y (ed) Bio-tribocorrosion in biomaterials and medical implants. Woodhead, Cambridge, pp 309–340
12. Ponthiaux P, Bayon R, Wenger F, Celis JP (2013) Testing protocol for the study of bio-tribocorrosion. In: Yan Y (ed) Bio-tribocorrosion in biomaterials and medical implants. Woodhead, Cambridge, pp 372–394
13. Mischler S, Munoz AI (2013) Wear of CoCrMo alloys used in metal-on-metal hip joints: a tribocorrosion appraisal. Wear 297: 1081–1094
14. Ortega-Saenz JA, Alvarez-Vera M, Hernandez-Rodriguez MAL (2013) Biotribological study of multilayer coated metal-on-metal hip prostheses in a hip joint simulator. Wear 301:234–242
15. Sheeja D, Tay BK, Nung LN (2004) Feasibility of diamond-like carbon coatings for orthopaedic applications. Diam Relat Mater 13:184–190
16. Wood RJK, Wharton JA (2011) Coatings for tribocorrosion protection. In: Landolt D, Mischler S (eds) Tribocorrosion of passive metals and coatings. Woodhead, Cambridge, pp 296–333
17. Luo X, Li X, Sun Y, Dong H (2013) Tribocorrosion behavior of S-phase surface engineered medical grade Co–Cr alloy. Wear 302:1615–1623
18. Espallargas N, Mischler S (2011) Dry wear and tribocorrosion mechanisms of pulsed plasma nitride N–Cr alloy. Wear 270: 464–471
19. Bazzoni A, Mischler S, Espallargas N (2013) Tribocorrosion of pulsed plasma-nitrided CoCrMo implant alloy. Tribol Lett 49:157–167
20. Gabriel Figueiredo Pina C, Dahm KL, Fisher J, Dearnley PA (2007) The damage tolerance of S-phase coated biomedical grade stainless steel. Wear 263:1081–1086
21. Dearnley PA, Aldrich-Smith G (2004) Corrosion-wear mechanisms of hard coated austenitic 316L stainless steel. Wear 256: 491–499
22. Sun Y (2013) Tribocorrosion behaviour of low temperature plasma carburized stainless steel. Surf Coat Technol 228:S342–S348
23. Dong H (2010) S-phase surface engineering of Fe–Cr, Co–Cr and Ni–Cr alloys. Int Mater Rev 55:65–98
24. Sun Y (2010) Production of nitrogen and carbon S phases in austenitic stainless steels by hybrid plasma surface alloying. Surf Eng 26:114–122

25. Dearnley PA, Namvar A, Hibberd GGA (1989) Some observations on plasma nitriding austenitic stainless-steel. In: Plasma surface engineering, volume 1, first international conference on plasma surface engineering 1988, Garmisch-Partenkirchen, DGM, Oberursel, Germany, pp. 219–226
26. Bourjot A, Foos M, Frantz C (1989) Chemical and structural characterization of M100-XNX thin-films prepared by magnetron reactive sputtering (M = AISI-310 stainless-steel, Molybdenum). In: Plasma surface engineering, volume 2, first international conference on plasma surface engineering 1988, Garmisch-Partenkirchen, DGM, Oberursel, Germany, pp. 777–784
27. Aldrich-Smith G, Teer DG, Dearnley PA (1999) Corrosion-wear response of sputtered CrN and S-phase coated austenitic stainless steel. Surf Coat Technol 116–119:1161–1165
28. Ohmori H, Mizutani M, Kaneeda T, Abe N, Okada Y, Moriyama S, Hisamori N, Nishimura N, Tsunashima Y, Tanaka J, Kuramoto K, Ezura A (2013) Surface generating process of artificial hip joints with hyper-hemispherical shape having higher smoothness and biocompatibility. CIRP Ann Manuf Technol 62:579–582
29. Sun Y, Haruman E (2011) Effect of electrochemical potential on tribocorrosion behaviour of low temperature plasma carburized 316L stainless steel in 1 M H_2SO_4 solution. Surf Coat Technol 205:4280–4290
30. Williams S, Tipper JL, Ingham E, Stone MH, Fisher J (2003) In vitro analysis of the wear, wear debris and biological activity of surface-engineered coatings for use in metal-on-metal total hip replacements. Proc Inst Mech Eng H 217:155–163
31. Leyland A, Matthews A (2000) On the significance of the *H*/*E* ratio in wear control: a nanocomposite coating approach to optimised tribological behaviour. Wear 246:1–11
32. Sinnett-Jones PE, Wharton JA, Wood RJK (2005) Micro-abrasion-corrosion of CoCrMo alloy in simulated artificial hip joint environments. Wear 259:898–909
33. Mallia B, Dearnley PA (2013) Exploring new W–B coating materials for the aqueous corrosion-wear protection of austenitic stainless steel. Thin Solid Films 549:204–215
34. Dearnley PA, Mallia B (2013) The chemical wear (corrosion-wear) of novel Cr based hard coated 316L austenitic stainless steel in aqueous saline solution. Wear 306:263–275
35. Maldonado SandraGuadalupe, Mischler Stefano, Catoni Marco, Chitty Walter-John, Falcand Carole, Hertz Dominique (2013) Mechanical and chemical mechanisms in the tribocorrosion of a Stellite type alloy. Wear 308:213–221
36. Mischler S (2008) Triboelectrochemical techniques and interpretation methods in tricorrosion: a comparative evaluation. Tribol Int 41:573–583
37. Watson SW, Friedersdorf FJ, Madsen BW, Gramer SD (1995) Methods of measuring wear-corrosion synergism. Wear 181–183: 476–484
38. Akonko A, Li DY, Ziomek-Moroz M (2005) Effect of cathodic protection on corrosive wear of 304 stainless steel. Tribol Lett 18:405–410
39. Bidiville A, Fvero M, Stadelmann P, Mischler S (2007) Effect of surface chemistry on the mechanical response of metals in sliding tribocorrosion systems. Wear 263:207–217
40. Favero M, Stadelmann P, Mischler S (2006) Effect of applied potential on the near surface microstructure of a 316L steel submitted to tribocorrosion in sulfuric acid. J Phys D 39:3175–3183
41. Pokhmurskii VI, Vynar VA, Vasyliv ChB, Ratska NB (2013) Effects of hydrogen exposure on the mechanical and tribological properties of α-titanium surfaces. Wear 306:47–50
42. Lee SJ, Lee YM, Du MF (2003) The polishing mechanism of electrochemical mechanical polishing technology. J Mater Process Technol 140:280–286